Antarctic Circumpolar Current impacts on internal wave life cycles

Stephanie Waterman[1], Amelie Meyer[2], Kurt Polzin[3], Alberto C. Naveira Garabato[4], and Katy Louise Sheen[5]

[1]University of British Columbia
[2]University of Tasmania
[3]Woods Hole Oceanographic Institution
[4]University of Southampton
[5]University of Exeter

November 24, 2022

Abstract

Major gaps exist in our understanding of the pathways between internal wave generation and breaking in the Southern Ocean, with important implications for the distribution of internal wave-driven mixing, its sensitivity to change, and the necessary ingredients of mixing parameterizations. Here we assess the dominant processes in internal wave evolution by characterizing wave and mesoscale flow scales based on full-depth measurements in a Southern Ocean mixing hot spot and a ray tracing calculation. The exercise highlights the importance of Antarctic Circumpolar Current (ACC) jets as a dominant influence on internal wave life cycles through advection, the modification of wave characteristics via wave-mean flow interactions, and the set-up of critical layers for both upward- and downward-propagating waves. Our findings suggest that it is important to represent mesoscale flow impacts in parameterizations of internal wave-driven mixing in the Southern Ocean.

Antarctic Circumpolar Current impacts on internal wave life cycles

S. Waterman[1], A. Meyer[2,3], K. L. Polzin[4], A. C. Naveira Garabato[5], and K. L. Sheen[6]

[1]Department of Earth, Ocean & Atmospheric Sciences, University of British Columbia, Vancouver, Canada.
[2]Institute for Marine and Antarctic Studies, University of Tasmania, Hobart, Tasmania, Australia
[3]Australian Research Council Centre of Excellence for Climate Extremes, University of Tasmania, Hobart, Tasmania, Australia
[4]Woods Hole Oceanographic Institution, Woods Hole, Massachusetts, USA
[5]University of Southampton, National Oceanography Centre, Southampton, UK
[6]University of Exeter, Penryn, UK

Key Points:

- In situ observations show internal wave-like coherent features in the Antarctic Circumpolar Current
- Wave and background flow scales suggest that horizontal advection and wave-mean flow interactions control the wave evolution
- Features are detected where the background flow shear is large and where ray tracing calculations suggest a critical layer scenario

Corresponding author: Stephanie Waterman, swaterman@eoas.ubc.ca

Abstract

Major gaps exist in our understanding of the pathways between internal wave generation and breaking in the Southern Ocean, with important implications for the distribution of internal wave-driven mixing, its sensitivity to change, and the necessary ingredients of mixing parameterizations. Here we assess the dominant processes in internal wave evolution by characterizing wave and mesoscale flow scales based on full-depth *in situ* measurements in a Southern Ocean mixing hot spot and a ray tracing calculation. The exercise highlights the importance of Antarctic Circumpolar Current (ACC) jets as a dominant influence on internal wave life cycles through advection, the modification of wave characteristics via wave-mean flow interactions, and the set-up of critical layers for both upward- and downward-propagating waves. Our findings suggest that it is important to represent mesoscale flow impacts in parameterizations of internal wave-driven mixing in the Southern Ocean.

1 Introduction

In the stratified ocean interior, turbulent mixing is primarily attributed to the breaking of internal waves. Currently, our understanding of this process is hampered by critical knowledge gaps concerning the pathways between internal wave generation and dissipation via wave breaking. These gaps are important to resolve for three key reasons: they determine how the spatial distribution of internal wave energy sources relate to that of internal wave-driven mixing; they impact the sensitivity of this mixing to changes in the wave field environment; and they define the necessary ingredients of parameterizations of internal wave-driven mixing for general circulation models.

It is generally assumed that internal waves in the ocean interior have originated from the upper-ocean mixed layer or the ocean floor, forced by winds at the surface or by the flow of tidal or geostrophic motions over rough topography. In both cases, internal waves can propagate away from their generation site before breaking and generating mixing. Observations of turbulent dissipation and internal wave-scale flow properties provide strong support for the perception that breaking internal waves are important for turbulent dissipation and mixing in the Southern Ocean interior (St. Laurent et al., 2013; Waterman et al., 2013; Sheen et al., 2013; Brearley et al., 2013; Meyer et al., 2015; Cusack et al., 2017). Here the contribution from bottom-sourced waves generated by the interaction of deep-reaching geostrophic jets and eddies with the bottom topography is thought to be especially significant (Nikurashin & Ferrari, 2013; de Lavergne et al., 2016).

There exist a number of thought-provoking results relating to internal wave-driven mixing in the Southern Ocean interior that raise important questions about the pathways to internal wave breaking in this unique environment. For example, theoretical predictions of the lee wave energy flux based on observed bottom flow speed, stratification and topography have been found to over-predict the observed near-bottom turbulent dissipation rate seen in different regimes of the ACC (Waterman et al., 2013; Sheen et al., 2013; Cusack et al., 2017). Similarly, finescale parameterization predictions for the dissipation rate based on the observed rate of energy transfer at internal wave scales have been found to systematically over-predict the observed near-bottom turbulent dissipation rate in regions of bottom wave generation (Sheen et al., 2013; Waterman et al., 2014; Takahashi & Hibiya, 2019). In addition, off-bottom maxima in observed dissipation rate vertical profiles in these regions (see Waterman et al., 2013; Sheen et al., 2013) do not match the vertical structure characteristically assumed in standard parameterizations for topographically-radiated internal wave-driven mixing (e.g. St. Laurent et al., 2002; Nikurashin & Ferrari, 2013).

A number of possible explanations for these thought-compelling mismatches have been suggested (Kunze & Lien, 2019), including the over-estimation of the lee wave energy flux because of the poor representation of near-bottom flows and/or small-scale bathymetry and/or flow blocking and splitting (Trossman et al., 2015; Nikurashin et al., 2014; Klymak, 2018); remote dissipation due to the downstream advection or cross-stream propagation of internal wave energy (Meyer et al., 2016; Zheng & Nikurashin, 2019; Kunze & Lien, 2019); the absorption of wave energy by the mean flow through wave-mean flow interactions/wave action conservation (Waterman et al., 2014; Kunze & Lien, 2019); and sampling biases in a heterogeneous turbulent field (Klymak, 2018). A growing number of results point to the importance of the mesoscale flow in playing an order-one role in the observed discrepancies and setting the structure of wave-driven mixing in the ACC. For example, we observe significant differences in the average vertical profiles of wave and turbulent properties inside ACC jets vs. outside ACC jets (Waterman et al., 2013; Sheen et al., 2013; Meyer et al., 2016). Further, we find an association of finescale parameterization over-prediction with large Froude numbers based on the vertical shear of the mesoscale flow (Sheen et al., 2013; Waterman et al., 2014). An association of prominent finescale parameterization over-prediction with background flows with systematic backing tendency (Waterman et al., 2014), as well as systematic trends in vertical profiles of wave polarization, shear-to-strain variance and turbulent dissipation inside ACC jets (Waterman et al., 2013; Sheen et al., 2013), each suggest that critical layer dynamics may play a systematic role at these special sites. Zheng & Nikurashin (2019) suggest that the advection of internal waves by the mean flow can significantly contribute to the reported difference between predicted wave generation and the observed energy dissipation, and Kunze & Lien (2019) argue that the transfer of lee wave energy back to the balanced flow through wave action conservation can account for a reduction in turbulent production by a factor of two. These varied results motivate further consideration of the implications of wave-mean flow interactions and other mesoscale flow influences on internal wave life cycles and, in turn, the magnitude and distribution of wave-induced mixing in this environment.

In this study, we exploit full-depth *in situ* measurements of internal wave-scale flow properties in a Southern Ocean mixing hot spot in which we expect elevated levels of internal wave activity owing to strong wind forcing and to the interaction of intense near-bottom flows with rough topography, as well as significant mesoscale flow influences associated with energetic ACC jets. We use these observations to identify and characterize both coherent internal wave-like signals, and the nature of these waves' background environment. Based on these characterizations, we evaluate the likely processes governing wave evolution through a characterization of timescales and a backward-in-time ray tracing calculation. Our work builds on that of Meyer et al. (2016), which characterized upper-ocean internal wave properties in this region using high-resolution hydrographic profiles from EM-APEX floats. Here, we extend this analysis using unique data in two significant ways: 1. expanding the wave characterization to full depth, allowing us to target bottom-generated waves closer to their generation site; and 2. probing plausible internal wave evolution pathways through a time-dependent ray tracing calculation in a realistic background flow and stratification environment.

2 Data and Methods

Our study is motivated by our identification of a number of coherent wave-like features in observations from the Southern Ocean Finestructure (SOFine) project, conducted in 2008 on the northern flank of the Kerguelen Plateau in the Indian Ocean sector of the

Southern Ocean. The survey site is characterized by the presence of multiple ACC frontal jets and moderately rough topography on horizontal scales of order 1-10 km. The jets' impingement on the topography is expected to be a strong local source of internal lee waves. In addition, strong wind forcing in the region is anticipated to be a significant surface source of near-inertial oscillations, which can then propagate into the ocean interior as near-inertial waves. Coherent wave-like features are identified both in the upper-ocean profiles of velocity and stratification collected by EM-APEX floats deployed in the region (see Meyer et al., 2016), as well as in full-depth conductivity-temperature-depth (CTD) and lowered acoustic Doppler current profiler (LADCP) profiles acquired during a ship-board survey (discussed here). These latter observations provide a unique opportunity to characterize the wave-like signals in the deep ocean in terms of internal wave kinematics, and to consider their relationship with the topography, stratification, and background ACC flow. Full details on the survey site, survey observations and data processing are given in Waterman et al. (2013).

The full-depth profiles of the horizontal velocity anomaly and the neutral surface height anomaly are systematically examined for the presence of coherent wave-like features, which are positively identified if all of a number of criteria on the observed wave signal are satisfied; see Section S1 of the Supporting Information for full details. Wave properties are then characterized by assuming that the feature is an internal wave (as in, for example, Müller et al., 1978; Polzin, 2008; Meyer et al., 2016) and applying linear wave theory; see Section S2 in the Supporting Information for a full description. In these calculations, we assume plane-wave internal waves propagating in a low Rossby number, Ro, low Froude number, Fr, geostrophically-balanced background flow correct to order (Ro, Fr) (see Polzin et al., 1996, for a discussion). To characterize properties of the background flow and stratification environment in which the coherent wave features are observed, CTD and LADCP profiles, as well as the satGEM projection (Meijers et al., 2011), are used. satGEM is a gravest empirical mode (GEM) projection of temperature and salinity fields in the Southern Ocean that, when combined with satellite altimetry, produces time-evolving temperature, salinity and velocity fields that approximate the mesoscale flow. The local background flow field is defined by smoothed variants of the measured velocity component vertical profiles, and the local background stratification is estimated via the adiabatic levelling method of Bray & Fofonoff (1981) applied to the measured N profile: see Section S3 in the Supporting Information for details. A comparison of the observed SOFine velocity profiles to those of the satGEM at relevant times and locations produces reasonable mesoscale structure agreement, endorsing our use of the satGEM product to provide background flow and stratification information at times and places where it is unavailable in the SOFine survey observations. The scales characterizing the wave features, and the background flow and stratification environment through which the waves propagate and evolve, are then combined to characterize timescales that indicate the relative importance of various processes influencing wave evolution: see Section S4 in the Supporting Information for details. Finally, the life history of observed waves is considered via a ray tracing calculation (*e.g.* Lighthill, 1978; Olbers, 1981; Sheen et al., 2015) using the satGEM projections to provide the time- and space-varying background flow and stratification fields. Full details of the calculation are provided in Section S5 in the Supporting Information.

3 Results

3.1 Wave characteristics

Based on the criteria defined in Section S1, we identify 7 downward-propagating and 14 upward-propagating coherent wave-like features in the 59 vertical profiles of LADCP and CTD observations. These wave-like features are commonly observed in the vicinity of the ACC frontal jets and/or in the eastern half of the survey domain (Figure 1); the latter is characterized by significantly rougher topography (see Waterman et al., 2013, their Figure 2d). Downward-propagating waves are observed exclusively at depths ranging from 1000 m to 1500 m. Upward-propagating waves are observed at a wide range of depths and heights above bottom, but are typically found within 500 to 1500 m of the seafloor (Table S1). Median wave scales computed as described in Section S2 characterize the downward-propagating waves as having typical vertical wavelengths of $\sim$140 m and horizontal wavelengths of $\sim$8 km, and upward-propagating waves as having vertical wavelengths of $\sim$120 m and horizontal wavelengths of $\sim$2 km. Significant variation amongst the individual features observed does exist, particularly in the vertical wavelength and frequency for upward-propagating waves (see Table S1 for standard deviations in wave properties). Downward-propagating waves exhibit a narrow range of intrinsic frequencies, all less than $1.25f$, where f is the local Corilois frequency. In contrast, upward-propagating waves have a much wider range of frequencies, with 5 of 14 waves having intrinsic frequencies greater than $2f$ (Fig. 1).

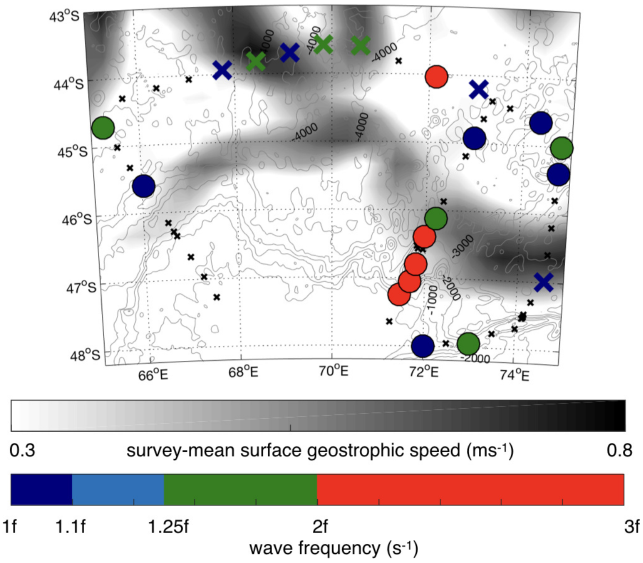

Figure 1. Location of observed coherent wave-like features (circles and enlarged **x**s), their direction of propagation (downward-propagating denoted by an **x**, upward-propagating by a circle), and their intrinsic frequency (color). For reference, the SOFine survey-mean surface geostrophic speed in the region computed from the Ssalto/Duacs altimeter products produced and distributed by the Copernicus Marine and Environment Monitoring Service (CMEMS) (`http://www.marine.copernicus.eu`), is shown in grey shading to outline the location of the ACC frontal jets during the survey period. Grey contours show the regional bathymetry in 500 m intervals from Smith and Sandwell ship-sounding bathymetry (Smith & Sandwell, 1997). Small black xs show the SOFine survey stations (refer to Waterman et al. (2013) for a full description of the SOFine survey).

3.2 Background environment

As already noted, the coherent wave-like features are typically observed in the vicinity of the ACC frontal jets that transected the survey domain. As such, background horizontal flow speeds at the locations of observed wave packets are typically moderate to large: 22 cm s^{-1} on average for downward-propagating waves, and 8 cm s^{-1} on average for upward-propagating waves. These background flow speeds are on average 10x (7x) larger than the diagnosed intrinsic horizontal group speeds of the waves for the case of downward-propagating (upward-propagating) waves. Large background flow horizontal speeds, combined with the horizontal wave scales estimated from the observed shear-to-strain ratio and velocity-buoyancy phase, imply significant mean flow-induced Doppler shifting of the waves' frequencies: median amplitudes of $1.0f$ for downward-propagating waves, and $0.8f$ for upward-propagating waves (Table S1).

Potentially important for these waves evolution is the nature of the background flow's vertical shear, strain and vorticity, expected to be elevated in the vicinity of ACC jets. LADCP measurements permit an *in situ* characterization of the larger-scale vertical shear in the vicinity of the coherent features identified (Table S1 and Figure 2). We find that downward-propagating features are always identified in positively-signed vertical shear (corresponding to decreasing background speed magnitude with depth), typically at depths that correspond to a transition from a more rapid decrease of background flow speed with depth above to a much more gradual decrease of background flow speed with depth below (Figure 2a). Upward-propagating coherent wave-like features are also characteristically observed near a transition in the background flow profile, with negatively-signed vertical shear (corresponding to an increase of background speed with depth toward the bottom) below and near-zero or positive vertical shear above (Figure 2b). Median magnitudes of vertical shear in the background flow in the vicinity of the features are $0.02N$ for down-going waves and $0.03N$ for up-going features respectively (Table S1), where N is the local background (*i.e.* smoothed) value of the buoyancy frequency. The satGEM product permits estimation of the large-scale flow strain and vorticity in the vicinity of identified features: we find median magnitudes of $0.1f$ and $0.1f$ for downward-propagating waves, and $0.06f$ and $0.02f$ for upward-propagating waves respectively (Table S1). These values are modest, but likely biased low by the coarse effective spatial resolution of the altimetric measurements (see, *e.g.*, Arbic et al., 2014). Elevated values of strain over vorticity imply that satGEM-derived estimates of the Okubo-Weiss parameter of the background flow are typically positive for both upward- and downward-propagating features (5 of 7 and 12 of 14 cases, respectively). In this scenario, the azimuth of the horizontal wave vector asymptotically points toward a direction solely determined by the geostrophic velocity gradient, and the magnitude of the wave vector is expected to exhibit exponential growth. Under these conditions, wave capture (Bühler & McIntyre, 2005) or the shrinking catastrophe (Jones, 1969) may be expected to play a significant role in the wave evolution.

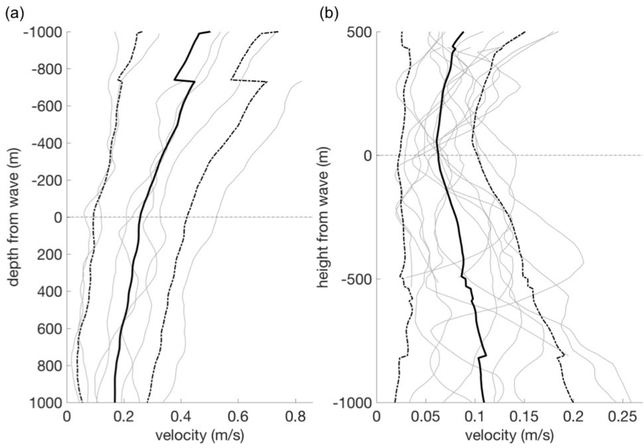

Figure 2. Background flow profiles in the vicinity of coherent wave-like features identified for all (a) downward-propagating and (b) upward-propagating features (light grey lines). The mean of all profiles is shown by the thick solid black line. The mean ± one standard deviation of the mean is shown by the thick dash-dotted black lines. Profiles are each centered around the observed depth/height of the coherent wave-like feature. Discontinuities in the mean and mean ± standard deviation profiles arise from changes in the number of profiles being averaged, a consequence of the profiles having differing 'depth from wave' extent.

3.3 Wave evolution

The exercise of using the observed wave and background flow and stratification scales to characterize various timescales associated with wave-mean flow interaction, advection and dissipation (Table S1 and Fig. 3) points to an order one importance of processes involving the large-scale flow in wave evolution. Of the 21 wave-like features identified, the characterization of these timescales indicates that advection is the dominant process (shortest timescale) in 67% of cases. Wave-mean flow interactions appear to be the dominant process for 24% of all features. Thus, local dissipation appears to be the dominant process in only 2 instances, or ∼10% of cases. As expected, we see that advection tends to dominate for downward-propagating low-frequency waves, while dissipation tends to dominate for upward-propagating high-frequency waves. Wave-mean flow interactions tend to be important mostly for downward-propagating waves, which are typically found in the large upper-ocean shear of the ACC. However, advection also dominates wave evolution for a near-equal number of downward-propagating features.

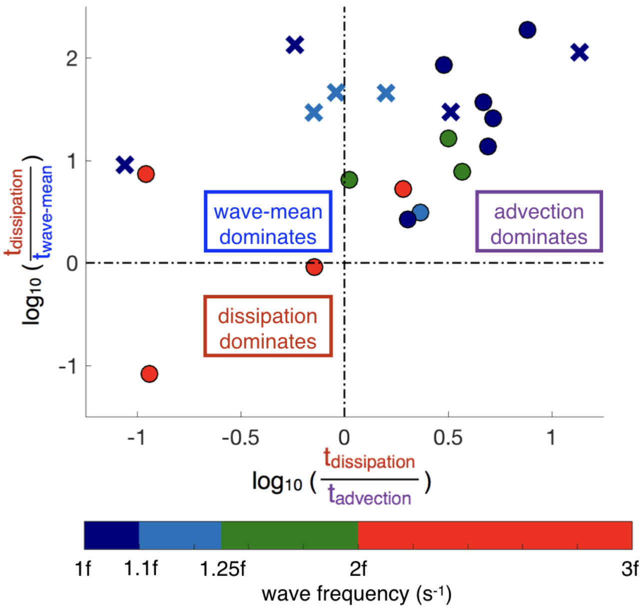

Figure 3. A comparison of timescales as defined in the Supporting Information for all coherent wave-like features. As in Fig. 1, downward-propagating features are denoted by **x**s and upward-propagating features by circles, and symbols are colored by their intrinsic wave frequency.

Further indications of order one roles played by the ACC in these waves' evolution are provided by the backwards-in-time ray tracing calculations. As described in Section S4, these afford an insightful picture of the plausible life cycle of the observed wave features prior to their observation. The illustration of key aspects of this evolution (Fig. 4) indicates an important role of the mesoscale flow in steering the trajectories of wave packets, as well as in generating non-local dissipation: downward-propagating coherent wave-like features are traced back to the base of the mixed layer in 2-12 days over which they travel a median distance of 160 km. However, background flow advection does not dominant in all cases: upward-propagating features have a much wider span of lifetimes, ranging from 0.1 days to 21 days, and in this time they travel a median distance of only 9 km. Features with the shortest lifetimes and most local dissipation cluster where the Polar Front passes over the rough topography of the plateau in the south-eastern part of the survey domain. Here, timescale analysis suggests that dissipation is the dominant process in these waves' evolution. A second compelling suggestion of an order one role played by the structure of the ACC in these waves' evolution is revealed in the visualizations of the wave packet trajectories in depth alongside the time-evolution of the wave frequency (Fig. 4b,c). These reveal that in the majority of cases (all downward-propagating features, and 9 of 12 upward-propagating features), the waves exhibit a common evolution from a higher-frequency, more vertical trajectory early in their life cycle (near the surface or near the bottom) to a frequency that approaches f and a trajectory that approaches horizontal at the time of observation. This evolution is consistent with the waves approaching a critical layer scenario in both downward- and upward-propagating cases. It should be noted that this result is likely to stem in part from the fact that we can detect coherent wave-like features in our observations only when they have sufficient amplitude. Nevertheless, this finding suggests that the ACC shear, and the critical layer situations that it can set up for both upward- and downward-propagating waves, may play an important role in setting the vertical profile of internal wave energy and internal wave-driven turbulent dissipation.

4 Summary and Discussion

In this study, we use *in situ* and satellite-derived measurements in a Southern Ocean mixing hot spot to characterize the scales of observed coherent internal wave-like features and the nature of these features' background environment, and further consider the dominant processes in internal wave evolution. Our results highlight the importance of the mesoscale flow in wave modification and in setting the pathway to internal wave-driven dissipation. Further, we suggest that our observations of large-amplitude coherent wave-like features stem from the wave packets' approach toward a critical layer scenario. Our findings indicate a significant role of mesoscale flow advection and wave-mean flow interactions in shaping the vertical profiles of internal wave-driven mixing and dissipation in the ACC, connecting sites of internal wave generation and breaking, and modulating the relationship between the internal wave energy flux and the local turbulent dissipation rate.

This work has several important limitations that need to be taken into consideration when assessing the implications of our results. First, with only a single hydrographic profile and a single velocity profile to characterize each wave feature, confidence limits on the estimated internal wave characteristics are unknown. Second, our knowledge of the three-dimensional background flow environment, based on the satGEM fields, is coarsely-resolved and subject to a number of assumptions. Of particular relevance is the expectation that the satGEM fields are likely to underestimate the influence of horizontal strain and vorticity on the waves' evolution. Third, the simple linear ray tracing model employed here does not capture the full range of wave-mean flow interactions at play in such a complex system. In particular, there are a number of scenarios in which the assumptions inherent to our linear ray tracing calculation may be violated, for example, in situations where the Wentzel-Kramers-Brillouin (WKB) approximation breaks down (*e.g.* Nault & Sutherland, 2008), where large-amplitude effects associated with the interaction of the waves and the wave-induced mean flow become significant (*e.g.* Brown et al., 2008), and, of particular relevance, where waves are evolving towards critical layer scenarios (see, *e.g.*, Booker & Bretherton, 1967; Jones, 1969; Olbers, 1981; Whitt & Thomas, 2013). Further, our formulation neglects additional processes such as instability mechanisms that may be important in transferring energy from larger-scale motions to dissipation scales (*e.g.* Thomas & Taylor, 2014). Finally, these observations are from a spatially-confined region in the Southern Ocean, and the applicability of these dynamics to the Southern Ocean generally remains an open question.

Given these limitations, it is appropriate to consider these characterizations of the wave field, the background flow environment and its influence on wave dynamics presented here as plausible scale estimates, and the ray tracing exercise to consider wave evolution as a heuristic technique. Some confidence in our wave parameter characterization is provided by the study of Meyer et al. (2016), who, by virtue of using EM-APEX float profile data in the region, have the luxury of exploiting consecutive profiles to characterize a single wave-like feature, and as such can estimate uncertainty in their derivation of wave parameters. They report that estimated uncertainties are small, and do not alter the interpretation of their results. Further, they document median wave parameters of similar scales to those reported here, within one mean standard deviation. Future observations targeting the assessment of wave properties and their local environment will be important to establish robustness of the characterizations presented here. We further recommend that the various effects and mechanisms not included in the simple linear ray tracing calculation discussed above be carefully considered in future work to determine whether their inclusion has a qualitative impact on findings presented here. Given that large rate-of-strain in the mesoscale flow is likely to play an important role in focusing wave-mean flow interaction, we specifically recommend that mesoscale rate-of-strain modulation of wave-mean flow interactions be explored in future with an appropriate data set. The upcoming Surface Water and Ocean Topography (SWOT) mission provides an exciting potential opportunity to do this.

Despite the above limitations and the need for further investigation, we argue that the big picture lessons suggested by the plausible scale estimates presented in this work are useful in guiding on-going research efforts on internal wave-driven mixing. Specifically, the identification of additional pathways and fates for internal wave energy suggested here may provide valuable perspectives from which to better understand the emerging relationships between spatial maps of internal wave energy sources and internal wave-driven dissipation and mixing (*e.g.* Waterhouse et al., 2014, and references therein), as well as the mismatches between our theoretical descriptions of the internal wave field and the distribution of turbulent dissipation identified in various recent studies (*i.e.* Waterman et al., 2013; Sheen et al., 2013; Nikurashin et al., 2014; Waterman et al., 2014; Cusack et al., 2017; Takahashi & Hibiya, 2019). By suggesting a plausible mesoscale flow modulation of the internal wave-driven mixing profile in this region, our results argue for a need to consider mesoscale flow influences in internal wave-driven mixing parameterizations.

Acknowledgments

The authors wish to thank the officers, crew, and scientific compliment aboard the RRS James Cook during cruise JC029. The SOFine project is funded by the UK Natural Environmental Research Council (NERC) (grant NE/G001510/1). The data used in the preparation of this manuscript are available on request from the British Oceanographic Data Centre (`http://www.bodc.ac.uk`). S.W is currently supported by the National Science and Engineering Research Council of Canada (NSERC) Discovery Grant Program (NSERC-2015-04866). A.M. acknowledges current support from the ARC Centre of Excellence for Climate Extremes (CE170100023) and previous support from the joint CSIRO-University of Tasmania Quantitative Marine Science (QMS) program. A.N.G. acknowledges the support of the Royal Society and the Wolfson Foundation.

References

Arbic, B. K., Müller, M., Richman, J. G., Shriver, J. F., Morten, A. J., Scott, R. B., … Penduff, T. (2014). Geostrophic turbulence in the frequency-wavenumber domain: Eddy-driven low-frequency variability. *J. Phys. Oceanogr.*, *44*(8), 2050–2069.

Booker, J. R., & Bretherton, F. P. (1967). The critical layer for internal gravity waves in a shear flow. *J. Fluid Mech.*, *27*(3), 513539.

Bray, N. A., & Fofonoff, N. P. (1981). Available potential energy for MODE eddies. *J. Phys. Oceanogr.*, *11*(1), 30-47.

Brearley, J. A., Sheen, K. L., Naveira Garabato, A. C., Smeed, D. A., & Waterman, S. (2013). Eddy-induced modulation of turbulent dissipation over rough topography in the Southern Ocean. *J. Phys. Oceanogr.*, *43*(1), 2288–2308.

Brown, G. L., Bush, A. B. G., & Sutherland, B. R. (2008). Beyond ray tracing for internal waves. II. Finite-amplitude effects. *Phys. Fluids*, *20*(10), 106602.

Bühler, O., & McIntyre, M. E. (2005). Wave capture and wave-vortex duality. *J. Fluid Mech.*, *534*, 67-95.

Cusack, J. M., Naveira Garabato, A. C., Smeed, D. A., & Girton, J. B. (2017). Observation of a large lee wave in the Drake Passage. *J. Phys. Oceanogr.*, *47*(4), 793-810.

de Lavergne, C., Madec, G., Le Sommer, J., Nurser, A. J. G., & Naveira Garabato, A. C. (2016). The impact of a variable mixing efficiency on the abyssal overturning. *J. Phys. Oceanogr.*, *46*(2), 663–681.

Jones, W. L. (1969). Ray tracing for internal gravity waves. *J. Geophys. Res.*, *74*(8), 2028-2033.

Klymak, J. M. (2018). Non-propagating form drag and turbulence due to stratified flow over large-scale abyssal hill topography. *J. Phys. Oceanogr.*, *48*(10), 2383-2395.

Kunze, E., & Lien, R.-C. (2019). Energy sinks for lee waves in shear flow. *J. Phys. Oceanogr.*, *49*(11), 2851-2865.

Lighthill, J. (1978). *Waves in fluids.* Cambridge University Press.

Meijers, A. J. S., Bindoff, N. L., & Rintoul, S. R. (2011). Frontal movements and property fluxes: Contributions to heat and freshwater trends in the Southern Ocean. *J. Geophys. Res. Oceans*, *116*(C8).

Meyer, A., Polzin, K. L., Sloyan, B. M., & Phillips, H. E. (2016). Internal waves and mixing near the Kerguelen Plateau. *J. Phys. Oceanogr.*, *46*(2), 417–437.

Meyer, A., Sloyan, B. M., Polzin, K. L., Phillips, H. E., & Bindoff, N. L. (2015). Mixing variability in the Southern Ocean. *J. Phys. Oceanogr.*, *45*(4), 966–987.

Müller, P., Olbers, D. J., & Willebrand, J. (1978). The Iwex spectrum. *J. Geophys. Res. Oceans*, *83*(C1), 479-500.

Nault, J. T., & Sutherland, B. R. (2008). Beyond ray tracing for internal waves. I. Small-amplitude anelastic waves. *Phys. Fluids*, *20*(10), 106601.

Nikurashin, M., & Ferrari, R. (2013). Overturning circulation driven by breaking internal waves in the deep ocean. *Geophys. Res. Lett.*, *40*(12), 3133-3137.

Nikurashin, M., Ferrari, R., Grisouard, N., & Polzin, K. (2014). The impact of finite-amplitude bottom topography on internal wave generation in the Southern Ocean. *J. Phys. Oceanogr.*, *44*(11), 2938-2950.

Olbers, D. J. (1981). The propagation of internal waves in a geostrophic current. *J. Phys. Oceanogr.*, *11*(9), 1224-1233.

Polzin, K. L. (2008). Mesoscale eddy-internal wave coupling. Part I: Symmetry, wave capture, and results from the Mid-Ocean Dynamics Experiment. *J. Phys. Oceanogr.*, *38*(11), 2556-2574.

Polzin, K. L., Oakey, N. S., Toole, J. M., & Schmitt, R. W. (1996). Fine structure and microstructure characteristics across the northwest Atlantic Subtropical Front. *J. Geophys. Res. Oceans*, *101*(C6), 14111-14121.

Sheen, K. L., Brearley, J. A., & Naveira Garabato, A. C. (2013). Rates and mechanisms of turbulent dissipation and mixing in the Southern Ocean: Results from the Diapycnal and Isopycnal Mixing Experiment in the Southern Ocean (DIMES). *J. Geophys. Res. Oceans*, *118*(6), 2774–2792.

Sheen, K. L., Brearley, J. A., Naveira Garabato, A. C., Smeed, D. A., Laurent, L. S., Meredith, M. P., ... Waterman, S. (2015). Modification of turbulent dissipation rates by a deep Southern Ocean eddy. *Geophys. Res. Lett.*, *42*(9), 3450-3457.

Smith, W. H. F., & Sandwell, D. T. (1997). Global sea floor topography from satellite altimetry and ship depth soundings. *Science*, *277*(5334), 1956–1962.

St. Laurent, L. C., Naveira Garabato, A. C., Ledwell, J. R., Thurnherr, A. M., Toole, J. M., & Watson, A. J. (2013). Turbulence and diapycnal mixing in Drake Passage. *J. Phys. Oceanogr.*, *42*(12), 2143-2152.

St. Laurent, L. C., Simmons, H. L., & Jayne, S. R. (2002). Estimating tidally driven mixing in the deep ocean. *Geophys. Res. Lett.*, *29*(23), 21-1-21-4.

Takahashi, A., & Hibiya, T. (2019). Assessment of finescale parameterizations of deep ocean mixing in the presence of geostrophic current shear: Results of microstructure measurements in the Antarctic Circumpolar Current region. *J. Geophys. Res. Oceans*, *124*(1), 135-153.

Thomas, L. N., & Taylor, J. R. (2014). Damping of inertial motions by parametric subharmonic instability in baroclinic currents. *J. Fluid Mech.*, *743*, 280294.

Trossman, D. S., Waterman, S., Polzin, K. L., Arbic, B. K., Garner, S. T., Naveira-Garabato, A. C., & Sheen, K. L. (2015). Internal lee wave closures: Parameter sensitivity and comparison to observations. *J. Geophys. Res. Oceans*, *120*(12), 7997-8019.

Waterhouse, A. F., MacKinnon, J. A., Nash, J. D., Alford, M. H., Kunze, E., Simmons, H. L., ... Lee, C. M. (2014). Global patterns of diapycnal mixing from measurements of the turbulent dissipation rate. *J. Phys. Oceanogr.*, *44*(7), 1854-1872.

Waterman, S., Naveira Garabato, A. C., & Polzin, K. L. (2013). Internal waves and turbulence in the Antarctic Circumpolar Current. *J. Phys. Oceanogr.*, *43*(2), 259–282.

Waterman, S., Polzin, K. L., Naveira Garabato, A. C., Sheen, K. L., & Forryan, A. (2014). Suppression of internal wave breaking in the Antarctic Circumpolar Current near topography. *J. Phys. Oceanogr.*, *44*(5), 1466–1492.

Whitt, D. B., & Thomas, L. N. (2013). Near-inertial waves in strongly baroclinic currents. *J. Phys. Oceanogr.*, *43*(4), 706-725.

Zheng, K., & Nikurashin, M. (2019). Downstream propagation and remote dissipation of internal waves in the Southern Ocean. *J. Phys. Oceanogr.*, *49*(7), 1873-1887.

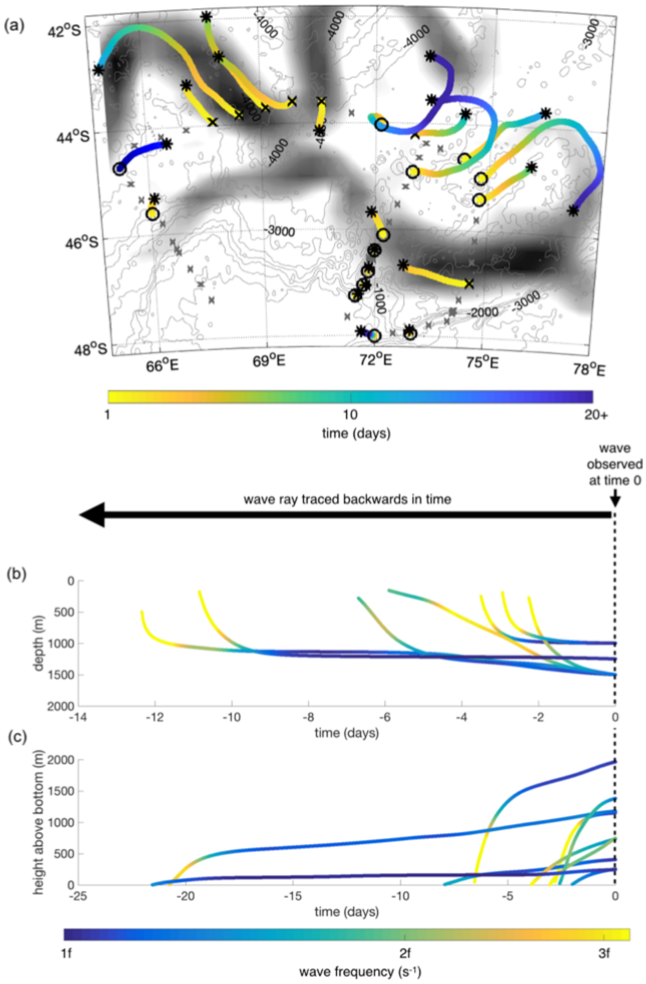

Figure 4. Plausible life histories of observed coherent wave-like features from backwards-in-time linear ray tracing calculations. (a) Horizontal trajectories of the wave packet colored by time before time observed. Mean surface geostrophic speed, regional bathymetry, survey stations and the location of observed downward-propagating *vs.* upward propagating wave-like features are indicated as in Fig. 1. Depth-time trajectories for (b) downward-propagating features and (c) select upward-propagating features. In both panels, the intrinsic frequency of the wave packet as a function of time is shown in color.

Supporting Information for "Antarctic Circumpolar Current impacts on internal wave life cycles"

S. Waterman[1], A. Meyer[2,3], K. L. Polzin[4], A. C. Naveira Garabato[5], and K. L. Sheen[6]

[1]Department of Earth, Ocean & Atmospheric Sciences, University of British Columbia, Vancouver, Canada.
[2]Institute for Marine and Antarctic Studies, University of Tasmania, Hobart, Tasmania, Australia
[3]Australian Research Council Centre of Excellence for Climate Extremes, University of Tasmania, Hobart, Tasmania, Australia
[4]Woods Hole Oceanographic Institution, Woods Hole, Massachusetts, USA
[5]University of Southampton, National Oceanography Centre, Southampton, UK
[6]University of Exeter, Penryn, UK

Contents

S1 Identification of wave features

The vertical profiles of density and horizontal velocity indicate the presence of many coherent wave-like features. These are visually identified in the profiles of the horizontal velocity anomaly and the neutral surface height anomaly, constructed by subtracting the observed profiles of horizontal velocity and neutral density from a smoothed variant of the measured profiles. The wave-like features occur as isolated signals with consistent amplitude and vertical wavelength over multiple wavelengths (for an example, see Figure S1). In this study, we systematically examine the SOFine CTD and LADCP pro-

Corresponding author: Stephanie Waterman, `swaterman@eoas.ubc.ca`

files for such features. We positively identify a so-called coherent wave-like feature if all of the following criteria are satisfied:

1. a coherent wave-like feature exhibits concurrent signals with a similar vertical wavelength in both the velocity anomaly and neutral surface height anomaly profiles;
2. the wave-like feature has a consistent or consistently varying wave amplitude and vertical wavelength for at least 1.5 vertical wavelengths;
3. a corresponding peak at a consistent vertical wavenumber is detected in all of the kinetic energy, potential energy and one component of the rotary motion spectra (the latter requires the feature to have a distinct polarization);
4. a matching peak in the spectral coherence between the relevant polarized component of the horizontal velocity and the buoyancy perturbation is observed.

As described in Section 3.1, the definition of these criteria results in the positive identification of 21 coherent wave-like features in the 59 vertical profiles of CTD and LADCP measurements.

We note that the features defined from the profile data in this manner are likely biased in at least two ways: first, toward waves with lower frequencies and large horizontal scales (as it is these waves that are visually discernible in the full-depth profiles); and second, toward waves with large enough amplitude to stand out from the background variability arising from the superposition of a range of waves and other oceanic motions. As such, our characterization should be considered as applying to a select subset of the full wave population present in the region.

S2 Characterization of wave properties

We characterize the coherent features identified by assuming that they are internal waves (as in, for example, Müller et al., 1978; Polzin, 2008; Meyer et al., 2016) and applying linear wave theory. In doing so, we assume that the waves can be described as small plane-wave perturbations about a background state of rest with a locally constant background stratification. We estimate the vertical wavenumber, m, from the peak in the total energy density spectrum (which, by the criteria defined above, is consistent with the vertical wavelength of the “wiggles” seen in vertical profiles of horizontal velocity and height anomalies, as well as the peak in the relevant component of the rotary motion spec-

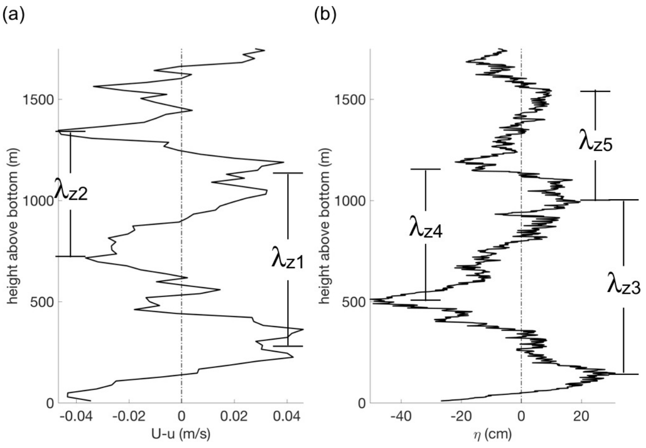

Figure S1. An example of a coherent wave-like feature seen in the vertical profiles of (a) the horizontal speed anomaly measured by the LADCP; and (b) the neutral surface height anomaly measured by the CTD. This particular example is from station 7 of the SOFine survey (see Fig. 1 of Waterman et al. (2013) for a station map). Here 2 and 3 vertical wavelengths of the feature are identified in the horizontal speed and height profiles respectively as indicated. We characterize the height of this feature as the midpoint of the vertical extent spanned by the wavelengths indicated. We characterize the vertical wavelength as the average value of all wavelengths indicated.

tra). The wave's vertical wavelength is subsequently estimated as $\lambda_z = \frac{2\pi}{m}$. The ratio of velocity variance in the clockwise- (E_{CW}) to counterclockwise- (E_{CCW}) rotating horizontal velocity components (called the rotary ratio) at this vertical scale is taken to indicate the direction of phase and energy propagation of the wave: for these Southern Hemisphere observations, a rotary ratio of less than 1 (i.e. $E_{CCW} > E_{CW}$) implies upward phase (and therefore downward energy) propagation, while a rotary ratio greater than 1 implies the opposite. Next we estimate the wave's intrinsic frequency, ω_0, from the ratio of kinetic energy, E_k, to potential energy, E_p, via $\omega_0 = f_0\sqrt{\frac{E_p(m)+E_k(m)}{E_k(m)-E_p(m)}}$. Here values of E_k and E_p are extracted from the energy spectra at the relevant vertical wavenumber m. We note that both instrumental noise, as well as 'noise' from other wave and non-wave motions is expected to bias this estimate high, we proceed with this caveat in mind. We subsequently estimate the wave's intrinsic period as $T_0 = \frac{1}{\omega_0}$. The waves horizontal wavenumber, k_H, is computed as $k_H = m\sqrt{\frac{\omega_0^2-f_0^2}{N^2-\omega_0^2}}$ (here f is the local value of the Coriolis frequency and N is the local background value of the stratification frequency, computed via the adiabatic leveling method of Bray & Fofonoff (1981) applied to the local N profile). This assumes an approximate dispersion relation for plane-wave internal waves propagating in a low Rossby number (Ro), low Froude number (Fr), geostrophically-balanced background flow correct to order (Ro, Fr) for all hydrostatic waves (Eqn. A3 in Polzin et al., 1996). It neglects terms involving second-order derivatives of the background which are small under a WKB approximation which is implicit when the plane wave solution is invoked, and further neglects terms proportional to the relative vorticity (order Ro), the thermal wind shear (order $BuFr$, where Bu is the Burger number) and the spatial derivatives of the mean advective terms order $\frac{Bu^2 Ro}{1+Bu^2}$). This is justified by the fact that wave features are characterized by low Ro and low Fr but a Bu that is order one (see Table S1). We note that the Bu O(1) limit is highly relevant in a wave capture scenario as waves asymptotically approach the aspect ratio of the mean flow, which tends to be $Bu \approx O(1)$ for the mesoscale. Here again, we expect noise to bias our estimate of k_H high. The wave's horizontal wavelength is then estimated as $\lambda_H = \frac{2\pi}{k_H}$. We obtain an estimate of the horizontal azimuth of the wave's wave vector, ϕ, from an estimate of the phase between the relevant rotary velocity component ($u-iv$ for an upward-propagating wave, and $u+iv$ for a downward-propagating wave, where u and v are the zonal and meridional velocity components respectively) and the buoyancy perturbation at the vertical wavenumber in question. From this phase estimate, we compute the horizontal wavenumber components, k and l, as $k = \pm k_H cos(\phi)$ (for upward- and downward-propagating waves respectively) and $l = -k_H sin(\phi)$. Finally, the components of the wave's group velocity, $\vec{c_{gH}}$, are estimated from the previously computed wave properties using internal wave relations derived from the gradients of the approximate dispersion relation: $c_{gx} = k\frac{(N^2-\omega_0^2)^2}{\omega_0 m^2 (N^2-f^2)}$, $c_{gy} = l\frac{(N^2-\omega_0^2)^2}{\omega_0 m^2 (N^2-f^2)}$, and $c_{gz} = \frac{(\omega_0^2-f^2)(N^2-\omega_0^2)^2}{\omega_0 m (N^2-f^2)}$. Our wave characterization follows that of Meyer et al. (2016). For more details, interested readers are referred to the discussion and references therein.

S3 Characterization of the background environment

We exploit the CTD and LADCP profiles to characterize properties of the background flow and stratification environment in which the coherent wave features are observed. The background flow field is defined by smoothed variants of the LADCP velocity component profiles, specifically by applying a sliding second-order polynomial regression with an increasing vertical fit window length ranging from ∼300 m at the surface to ∼800 m at depth. The goal of the smooth fit is to eliminate variability on vertical scales

	Downward-going			Upward-going		
	mean	median	std	mean	median	std
1. WAVE PROPERTIES						
depth (for downward)/height (for upward) (m)	1321	1500	238	932	949	607
average vertical wavelength (m)	141	143	42	132	120	68
horizontal wavelength (km)	10	8	9	4	2	6
intrinsic frequency/f	1.1	1.1	0.1	2.2	1.2	3.0
intrinsic group velocity (horizontal),CgH	2.0	2.1	1.1	1.7	1.2	1.4
intrinsic group velocity (vertical) (cm/s)	-0.05	-0.04	0.04	0.2	0.1	0.3
2. BACKGROUND PROPERTIES						
horizontal speed, U (cm/s)	0.22	0.13	0.24	0.08	0.05	0.07
U/CgH	3.8	9.6	3.1	1.4	6.6	0.6
|vertical shear/N|	0.02	0.02	0.01	0.05	0.03	0.1
|strain/f|	0.1	0.1	0.07	0.08	0.06	0.01
|vorticity/f|	0.1	0.1	0.04	0.04	0.02	0.04
|Doppler shift/f|	2.3	1.0	3.7	3.3	0.8	7.6
3. TIMESCALES						
e-folding for *m* (days)	29	7	51	67	25	87
e-folding for *k* (days)	9	3	15	225	4	786
e-folding for *l* (days)	3	2	3	126	2	429
dissipation (days)	4	1	7	3	1	6
advection (days)	2	2	1	3	3	2
distance in 1 dissipation time (km)	48	22	81	33	8	62
4. RAY TRACING RESULTS						
lifetime (days)	7	6	4	12	12	12
horizontal distance (km)	188	160	129	70	70	70
5. NON-DIMENSIONAL PARAMETERS						
Rossby number, Ro	0.1	0.1	0.04	0.04	0.02	0.04
Froude number, Fr	0.02	0.02	0.01	0.05	0.03	0.1
Burger Number, Br	0.5	0.4	0.2	1.0	0.7	0.7

Table S1. Statistics summarizing the wave properties, background flow properties, timescales, ray tracing calculation results and non-dimensional parameters for all wave-like features identified. Here the Rossby number, Ro, is computed as $Ro = \frac{\zeta}{F}$ where ζ is the vertical component of the large-scale flow vorticity and f is the local Corilois frequency, the Froude number, Fr, is computed as $Fr = \frac{\frac{\partial \vec{U}}{\partial z}}{N}$ where $\vec{U}$ is the large-scale horizontal velocity and N is the background stratification, and the Burger number, Bu, is computed as $Bu = \frac{N^2 k_H^2}{f^2 m^2}$.

of a few hundred meters and less, while maintaining the large-scale structure associated with the ACC jets. Results are insensitive to the specific choice of the smoothing parameters, as long as this qualitative goal is achieved. The background stratification is defined by a smooth N profile, constructed via the adiabatic leveling method of Bray & Fofonoff (1981) applied to the local N profile with a pressure range of adiabatic leveling of 400 decibars. Again, results are qualitatively insensitive to this choice provided it remains on the order of hundreds of decibars. We use these constructed profiles to characterize the magnitude of the background flow velocity components, U and V, the magnitude of the background vertical shear, and the local background stratification and its vertical gradient in the vicinity of each observed coherent wave packet.

Our consideration of the background flow impacts on three-dimensional wave evolution is also dependent on the magnitude of the horizontal velocity gradients of the background flow. This information is unavailable from the SOFine station data: the station spacing (typically 40 km) is relatively coarse, and often provides velocity gradient information in only one horizontal direction. As such, here we rely on velocity information from satGEM (Meijers et al., 2011), a gravest empirical mode (GEM) projection of temperature and salinity fields in the Southern Ocean that, when combined with satellite altimetry, produces time-evolving temperature, salinity and velocity fields at 7-day intervals on a $1/3^o$ grid. A comparison of the observed SOFine velocity profiles to those of the satGEM at relevant times and locations produces reasonable mesoscale structure agreement, endorsing our use of the satGEM product to provide background flow and stratification information at times and places where it is unavailable in the SOFine survey observations.

S4 Timescale characterization of wave evolution

The scales characterizing the wave features, and the background flow and stratification environment through which the waves propagate and evolve, can be combined to characterize timescales that indicate the relative importance of various processes influencing wave evolution. Here we characterize the relative importance of: 1. the wave scale's modification due to the background flow's shear, strain and stratification; 2. the waves horizontal translation due to intrinsic propagation and mean flow advection; and 3. the wave's dissipation. We do this by computing the following timescales:

1. the wave-mean flow interaction timescale, $\tau_{\text{wave-mean}}$, characterizing the time it takes for the various wavenumber components of the wave to change significantly (specifically by e^{-1}) due to interaction with the background flow's shear, strain and stratification gradients. $\tau_{\text{wave-mean}}$ is computed as $\tau_{\text{wave-mean}k} = \frac{k}{-k\frac{\partial U}{\partial x} - l\frac{\partial V}{\partial x}}$, $\tau_{\text{wave-mean}l} = \frac{l}{-k\frac{\partial U}{\partial y} - l\frac{\partial V}{\partial l}}$ and $\tau_{\text{wave-mean}m} = \frac{m}{-k\frac{\partial U}{\partial z} - l\frac{\partial V}{\partial z} - \frac{\partial \sigma}{\partial z}}$ for the k, l and m components of the wavenumber, respectively. Here $\frac{\partial \sigma}{\partial z}$, the vertical gradient of the wave's intrinsic frequency, is given by $\frac{\partial \sigma}{\partial z} = N\frac{\partial N}{\partial z}\frac{k_H^2}{m^2}[\frac{N^2k_H^2+f^2m^2}{m^2}]^{1/2}$.
2. the advection timescale, $\tau_{\text{advection}}$, characterizing the time it would take for the wave to travel away from the local environment due to both intrinsic wave propagation and advection by the background flow. $\tau_{\text{advection}}$ is computed as $\tau_{\text{advection}} = \frac{L_{Rd}}{\vec{U}+\vec{c_{gH}}}$,

where L_{Rd} is set to be a characteristic value for the local first-baroclinic Rossby radius of deformation at these latitudes, $L_{Rd} = 15$ km.

3. the dissipation timescale, τ_ϵ, characterizing the time it would take for the observed wave energy to dissipate, given the local microstructure measurement of the turbulent kinetic energy dissipation rate, ϵ (see Waterman et al. (2013) for a full description of the microstructure measurements associated with the SOFine finescale measurements discussed here). τ_ϵ is computed as $\tau_\epsilon = \frac{E(m)}{\epsilon}$, where $E(m) = E_p(m) + E_k(m)$, the total observed energy at the vertical wavenumber m in question. We note that, in general, the local measure of the dissipation rate is not that associated with the breaking of a single wave but rather the rate of energy transfer through the inertial subrange. Here we use the microstructure measure of ϵ as an appropriate order of magnitude estimate for the dissipation rate of the coherent feature energy.

An internal wave with a dissipation timescale shorter than its advection timescale will undergo local dissipation. Conversely, if the advection timescale is less than the dissipation timescale, we expect that the dissipation of the wave will be remote. The amplitude of the wave-mean flow interaction timescale relative to the dissipation timescale indicates the extent to which wave-mean flow interactions can play a role in disrupting the simple picture of a downscale energy cascade via wave-wave interactions assumed by, for example, finescale parameterizations. If $\tau_{\text{wave-mean}_m}$ is short relative to the dissipation timescale, the influence of the background flow's vertical shear will play a significant role in the evolution of the wave's vertical scale (either accelerating or opposing the downscale cascade by wave-wave interactions). If $\tau_{\text{wave-mean}_k}$ and $\tau_{\text{wave-mean}_l}$ are relatively short, the waves evolution must be considered as fundamentally 3-dimensional.

S5 Ray tracing calculations

The propagation of internal wave packets, and the evolution of their properties along a ray path for a specific background stratification and velocity field, may be mapped using ray tracing techniques (*e.g.* Lighthill, 1978; Olbers, 1981; Sheen et al., 2015). In addition to their intrinsic propagation, internal wave rays are also advected by the background horizontal current, $\vec{U}(x, y, z, t) = U(x, y, z, t) + V(x, y, z, t)$, and distorted by the local current shears, $\frac{\partial \vec{U}(x,y,z,t)}{\partial x}$, $\frac{\partial \vec{U}(x,y,z,t)}{\partial y}$ and $\frac{\partial \vec{U}(x,y,z,t)}{\partial z}$, and background stratification gradient, $\frac{\partial N(x,y,z,t)}{\partial z}$, along their ray path. Note, consistent with our approximation to the dispersion relation, we neglect the horizontal gradients of intrinsic frequency in the ray tracing equations for the evolution of the wave's wavenumber on the basis that the term arising from the thermal wind shear is small in the WKB limit. This is appropriate as the life cycle of $Bu \approx O(1)$ and larger waves is controlled by variations in the Doppler shift rather than having behavior that depends strongly upon the background relative vorticity. In this work we consider a plausible life history of the observed coherent wave packets by ray-tracing them backwards-in-time from the time and location of observation. We use the satGEM data to provide the time- and space-varying background flow and stratification fields. We use the ray tracing model to track the temporal evolution of the wave's position and characteristics using finite-differencing, with the wave position, wavenumber and frequency being updated on 10-minute time steps. We also record the temporal evolution of background flow and stratification properties along the ray path, in order to document the evolving influence of the background environment on the wave's evolution. The model is run until the wave packet intersects the seafloor or the base of the mixed layer, a period that ranged from 0.1 to 21 days.

References

Bray, N. A., & Fofonoff, N. P. (1981). Available potential energy for MODE eddies. *J. Phys. Oceanogr.*, *11*(1), 30-47.

Lighthill, J. (1978). *Waves in fluids.* Cambridge University Press.

Meijers, A. J. S., Bindoff, N. L., & Rintoul, S. R. (2011). Frontal movements and property fluxes: Contributions to heat and freshwater trends in the Southern Ocean. *J. Geophys. Res. Oceans*, *116*(C8).

Meyer, A., Polzin, K. L., Sloyan, B. M., & Phillips, H. E. (2016). Internal waves and mixing near the Kerguelen Plateau. *J. Phys. Oceanogr.*, *46*(2), 417–437.

Müller, P., Olbers, D. J., & Willebrand, J. (1978). The Iwex spectrum. *J. Geophys. Res. Oceans*, *83*(C1), 479-500.

Olbers, D. J. (1981). The propagation of internal waves in a geostrophic current. *J. Phys. Oceanogr.*, *11*(9), 1224-1233.

Polzin, K. L. (2008). Mesoscale eddy-internal wave coupling. Part I: Symmetry, wave capture, and results from the Mid-Ocean Dynamics Experiment. *J. Phys. Oceanogr.*, *38*(11), 2556-2574.

Polzin, K. L., Oakey, N. S., Toole, J. M., & Schmitt, R. W. (1996). Fine structure and microstructure characteristics across the northwest Atlantic Subtropical Front. *J. Geophys. Res. Oceans*, *101*(C6), 14111-14121.

Sheen, K. L., Brearley, J. A., Naveira Garabato, A. C., Smeed, D. A., Laurent, L. S., Meredith, M. P., ... Waterman, S. (2015). Modification of turbulent dissipation rates by a deep Southern Ocean eddy. *Geophys. Res. Lett.*, *42*(9), 3450-3457.

Waterman, S., Naveira Garabato, A. C., & Polzin, K. L. (2013). Internal waves and turbulence in the Antarctic Circumpolar Current. *J. Phys. Oceanogr.*, *43*(2), 259–282.